AGU PUBLICATIONS

Geophysical Research Letters

RESEARCH LETTER
10.1002/2017GL076622

Key Points:
- A novel Bayesian fusion is applied to infer GPP and TER from the global carbon budget equation
- Growth trends of GPP and TER are reduced after optimization
- TER growth stalled after Pinatubo eruption and during the hiatus period

Supporting Information:
- Supporting Information S1

Correspondence to:
W. Li,
wei.li@lsce.ipsl.fr

Citation:
Li, W., Ciais, P., Wang, Y., Yin, Y., Peng, S., Zhu, Z., … Piao, S. (2018). Recent changes in global photosynthesis and terrestrial ecosystem respiration constrained from multiple observations. *Geophysical Research Letters*, *45*, 1058–1068. https://doi.org/10.1002/2017GL076622

Received 9 JUN 2017
Accepted 5 JAN 2018
Accepted article online 8 JAN 2018
Published online 26 JAN 2018

Recent Changes in Global Photosynthesis and Terrestrial Ecosystem Respiration Constrained From Multiple Observations

Wei Li[1], Philippe Ciais[1], Yilong Wang[1], Yi Yin[1], Shushi Peng[1,2], Zaichun Zhu[2], Ana Bastos[1], Chao Yue[1], Ashley P. Ballantyne[3], Grégoire Broquet[1], Josep G. Canadell[4], Alessandro Cescatti[5], Chi Chen[6], Leila Cooper[3], Pierre Friedlingstein[7], Corinne Le Quéré[8], Ranga B. Myneni[5], and Shilong Piao[2]

[1]Laboratoire des Sciences du Climat et de l'Environnement/IPSL, CEA-CNRS-UVSQ, Université Paris-Saclay, Gif-sur-Yvette, France, [2]Department of Ecology, College of Urban and Environmental Sciences, Peking University, Beijing, China, [3]Department of Ecosystem and Conservation Science, University of Montana, Missoula, MT, USA, [4]Global Carbon Project, CSIRO Oceans and Atmosphere, Canberra, ACT, Australia, [5]Institute for Environment and Sustainability, Joint Research Centre, European Commission, Ispra, Italy, [6]Department of Earth and Environment, Boston University, Boston, MA, USA, [7]College of Engineering, Mathematics and Physical Sciences, University of Exeter, Exeter, UK, [8]Tyndall Centre for Climate Change Research, University of East Anglia, Norwich, UK

Abstract To assess global carbon cycle variability, we decompose the net land carbon sink into the sum of gross primary productivity (GPP), terrestrial ecosystem respiration (TER), and fire emissions and apply a Bayesian framework to constrain these fluxes between 1980 and 2014. The constrained GPP and TER fluxes show an increasing trend of only half of the prior trend simulated by models. From the optimization, we infer that TER increased in parallel with GPP from 1980 to 1990, but then stalled during the cooler periods, in 1990–1994 coincident with the Pinatubo eruption, and during the recent warming hiatus period. After each of these TER stalling periods, TER is found to increase faster than GPP, explaining a relative reduction of the net land sink. These results shed light on decadal variations of GPP and TER and suggest that they exhibit different responses to temperature anomalies over the last 35 years.

1. Introduction

Gross primary production (GPP) and terrestrial ecosystem respiration (TER) are the two largest fluxes of CO_2 between the atmosphere and biosphere. An accurate quantification of the variability and trends of these fluxes is crucial to understand observed changes in the net land carbon sink. Global data-driven GPP estimates have been provided by up-scaling measurements from eddy covariance sites through model tree ensembles (Beer et al., 2010; Jung et al., 2011) and by translating spaceborne observations of the fraction of absorbed photosynthetically active radiation (fAPAR) using empirical light use efficiency (LUE) models (Zhao et al., 2005). Spaceborne measurements of Sun-induced chlorophyll fluorescence also offer the potential to constrain GPP variability, but the limited length of the time series prevents a proper assessment of the temporal trends (Duveiller & Cescatti, 2016; Frankenberg et al., 2011; Guanter et al., 2012; Joiner et al., 2013). However, discrepancies exist between the global mean GPP values from different data products (e.g., 123 ± 8 PgC yr^{-1} during 1998–2005 in Beer et al., 2010, compared to 109 PgC yr^{-1} from 2001 to 2003 in Zhao et al., 2005). The observed temporal trend of GPP is also uncertain (Anav et al., 2015; Huang et al., 2015) probably because the long-term CO_2 fertilization on photosynthesis is only partly incorporated into LUE models and also partly accounted for in eddy-covariance up-scaling products based on short-term measurements, remote sensing observations, and climate data products.

In contrast to GPP, there are very few global products of TER, due to the difficulty in up-scaling heterogeneous site-level measurements (Luo et al., 2016). The information content of satellite observations to constrain TER is also limited (Jung et al., 2011). To our knowledge, there is only one global soil respiration database compiled by Bond-Lamberty and Thomson (2010) from 1,434 point-scale field measurements. A positive temporal trend of global soil respiration between 1989 and 2008 was found in this data set, but with a large uncertainty. As an alternative to direct observations, TER can be indirectly constrained from the mass balance of the net land sink, GPP, and fire emissions (FR).

Decadal variability of the net carbon fluxes in the global carbon budget, i.e., land and ocean sinks, land use change emissions, and fossil fuel emissions, was studied by Li et al. (2016) using a Bayesian method. This study goes one step further by analyzing the decadal variability of GPP and TER constrained by long-term observations. Here we combine different observational data sets of global gross and net carbon fluxes (Ciais et al., 2013; Le Quéré et al., 2015) in a Bayesian fusion framework to infer decadal changes of GPP and TER. Specifically, we decompose the net land carbon flux (B + L), where B is the net carbon sink over lands not affected by land use change and L is land use change emission, into gross fluxes, according to B + L = GPP + TER + FR. We focus here on gross fluxes and thus take (B + L) as a single observed constraint in the inversion system, instead of considering separate estimates of B and L. The Bayesian fusion method combines prior values of fluxes from models with observational data sets to provide optimal estimates. In our study, GPP, TER, and FR are constrained by their own related observation-based data (Figure S1 in the supporting information), but also indirectly by the observation of B + L. Because most global observation-based data sets are available after 1980 only, the Bayesian fusion is applied on 5 year intervals from 1980 to 2014 to keep observational constraints efficient and yet make it possible to study quasi-decadal temporal variability in land fluxes. Furthermore, looking at 5 year intervals reduces the interannual variability of net terrestrial carbon exchange that we know is due to temperature and precipitation anomalies associated with El Niño–Southern Oscillation (Betts et al., 2016).

2. Materials and Methods

2.1. Prior and Constraining Data

The control fluxes to be optimized are (1) fossil fuel and cement emissions (F), (2) ocean sink (O), (3) fire emissions (FR), (4) mean GPP (G_0) and TER (T_0) during the period of 2005–2009, and (5) GPP and TER changes (ΔGPP and ΔTER) over consecutive 5 year periods. The prior F estimates are from four inventories, and O are from biogeochemistry models, which were also used in Li et al. (2016). Prior distributions of FR, G_0, T_0, ΔGPP, and ΔTER are the ensemble means from the TRENDY v2 dynamic global vegetation models (DGVMs; Table S1) (Best et al., 2011; Clark et al., 2011; Ito & Inatomi, 2012; Jain & Yang, 2005; Kato et al., 2013; Krinner et al., 2005; Oleson et al., 2013; Reick et al., 2013; Sitch et al., 2003, 2015; Smith et al., 2001; Stocker et al., 2014; Zaehle & Friend, 2010; Zeng et al., 2005). The priors of these fluxes are shown in Table S2.

Observational data sets (Table S3) compiled (Heil et al., 2010; Jacobson et al., 2007; Pan et al., 2011; Rödenbeck et al., 2013, 2015; Van Der Werf et al., 2010; Zhao, Running, & Nemani, 2006) to constrain these prior estimates are (1) 5 year averaged CO_2 growth rate from NOAA/Earth System Research Laboratory (ESRL) atmospheric stations (Ballantyne et al., 2015; NOAA/ESRL, 2015); (2) 5 year averaged growth rate of O_2/N_2 in the atmosphere from the Scripps O_2 Program (Keeling & Manning, 2014); (3) five observation-driven estimates of O (Khatiwala et al., 2009; Landschützer et al., 2014; McNeil et al., 2003; Rödenbeck et al., 2014; Steinkamp & Gruber, 2013); (4) decadal mean estimates of B + L from the Regional Carbon Cycle Assessment and Processes regional budget publications, mainly based on land carbon storage change inventories (see Table S3 in Li et al., 2016); (5) GPP data sets from the Moderate Resolution Imaging Spectroradiometer (MODIS) data-driven model over 2001–2014 (Zhao et al., 2005), the Max Planck Institute for Biogeochemistry (MPI-BGC) product using FLUXNET measurements over 1982–2011 (Jung et al., 2011) and the Breathing Earth System Simulator (BESS) data-driven model (Jiang & Ryu, 2016); (6) a proxy of relative changes of GPP, given by growing season integrated leaf area index (LAI) variations from three LAI data sets (Liu et al., 2012; Xiao et al., 2014; Zhu et al., 2013); (7) a proxy of the TER trend from the compilation of field measurements of soil respiration (Bond-Lamberty & Thomson, 2010); and (8) 5 year mean observation-based FR values from Global Fire Emissions Database Version 4.1s (Giglio et al., 2013) and from the Reanalysis of the Tropospheric chemical composition reconstruction (Schultz et al., 2008). Data sets that represent mean values for a period longer than 5 years constrain the mean fluxes over this period rather than individual 5 year intervals.

The three LAI data sets used as proxies of GPP changes are from Global Inventory Modeling and Mapping Studies (GIMMS) (Zhu et al., 2013), Global Land Surface Satellites (GLASS) (Xiao et al., 2014), and Long-term Global Mapping (GLOBMAP) LAI (Liu et al., 2012). They are based on measurements from the same space-borne instruments (MODIS and advanced very high resolution radiometer) but inferred with different algorithms (Zhu et al., 2013). Error correlations between these three LAI data sets are challenging to

quantify, but we cannot assume that the LAI products are independent. Similarly, error correlations between the three GPP data sets (Jiang & Ryu, 2016; Jung et al., 2011; Zhao et al., 2005) are difficult to estimate, but they are not independent either, for instance, because they use similar climate fields and/or remote sensing fields but different algorithms. In this study, we test the nine possible combinations of LAI and GPP as constraining data, i.e., a combination of only one single GPP product and one single LAI products in each test, to avoid not correctly accounting for the potential correlations in their uncertainties. Uncertainties in this study refer to 1-σ Gaussian errors, and CO_2 emissions to the atmosphere are defined as positive.

In the Bayesian inference system, we define the "control variables" $\mathbf{x}$ as 5 year mean values of F, O, FR, ΔGPP, and ΔTER from 1980 to 2014 and G_0 and T_0 during 2005–2009. These control variables are connected to observation data sets through the observation operator H. The Bayesian inference system allows us to solve for the optimal estimate of the control variables $\mathbf{x^a}$ that fit both the prior estimates with their error statistics $\mathbf{B}$ and the constraining data $\mathbf{y^0}$ with their error statistics $\mathbf{R}$, by minimizing the cost function (Tarantola, 2005):

$$J(\mathbf{x}) = \frac{1}{2}\left[\left(\mathbf{x}-\mathbf{x^b}\right)^{\mathrm{T}}\mathbf{B}^{-1}\left(\mathbf{x}-\mathbf{x^b}\right) + \left(\mathbf{y^0} - H[\mathbf{x}]\right)^{\mathrm{T}}\mathbf{R}^{-1}\left(\mathbf{y^0} - H[\mathbf{x}]\right)\right] \quad (1)$$

where the superscripts T and "−1" indicate the transpose and inverse of a matrix, respectively. The full configuration of the system is detailed in Text S1.

Five sensitivity tests were performed to evaluate the robustness of our results (see details in Text S2): (1) using two alternative FR data sets (GFAS (Kaiser et al., 2012) and GICC (Mieville et al., 2010)), (2) removing the soil respiration constraint, (3) removing LAI constraints, (4) removing influence of prior GPP and TER trends, and (5) adding the leaf-scale CO_2 effects on LUE.

2.2. Anomaly of Carbon Fluxes and Climate Conditions

Anomalies of 5 year fluxes were calculated by removing a linear trend over the seven 5 year periods from 1980 to 2014. The same method was applied to derive anomalies of temperature from GHCN_CAMS (Fan & van den Dool, 2008) and CRU3.23 (Harris et al., 2014), precipitation from CRU3.23 (Harris et al., 2014), water availability index (WAI) (Jung et al., 2017; Tramontana et al., 2016), and soil moisture from Climate Prediction Center (CPC) (Fan & van den Dool, 2004) and the European Space Agency-Climate Change Initiative satellite products (Dorigo et al., 2010). The ordinary-least-squares method was applied in the multiple regressions of TER anomalies against GPP anomalies and climate variable anomalies.

3. Results

3.1. Optimized Carbon Fluxes

The optimized mean GPP and TER estimates are lower by about 18 PgC yr^{-1} compared to prior values (Figure 1a and Table S2), giving best estimates of GPP = −119 ± 12 PgC yr^{-1} and TER = 115 ± 12 PgC yr^{-1} during 1980–2014. Note that here we used the mean values from the nine combinations for the synthesis results (unless otherwise specified), the values for each combination being provided in Table S4. The reduction of optimized GPP and TER magnitude from priors is caused by observation-based GPP estimates being lower than the prior from DGVMs (see values in Tables S2 and S3). For example, the observation-based GPP during 2000–2004 is −111 ± 21, −119 ± 32, and −122 ± 25 PgC yr^{-1}, respectively, from MODIS, MPI-BGC, and BESS, compared to the prior from DGVM models of −140 ± 37 PgC yr^{-1}. Because the sum of TER and GPP must scale to the observed net land flux, mean TER is also lower than the prior. The uncertainties in GPP and TER are reduced by 67% from the prior values from DGVMs for each different combination of GPP and LAI data sets. The optimized FR is 2.3 ± 0.49 PgC yr^{-1} during 1980–2014, with an SD of 0.30 PgC yr^{-1} across the different 5 year periods (Figure 1a). This estimate is 19% less than the prior, and its uncertainty is reduced by 49% (Figure 1b), reflecting the fact that both observation-based FR data sets are lower than the priors from the DGVMs (Table S3). Posterior FR shows a significantly declining trend over the entire period ($p < 0.05$) at a rate of −0.019 PgC yr^{-2}. The uncertainty reductions for F, O, and B + L (Figures 1c and 1d) are similar with those obtained by Li et al. (2016), who used the same observational constraints for net fluxes.

The nine different combinations of LAI relative trends and GPP observational constraints result in different optimized GPP and TER (coefficient of variation = 3.9% and 4.0%). The optimized GPP during 1980–

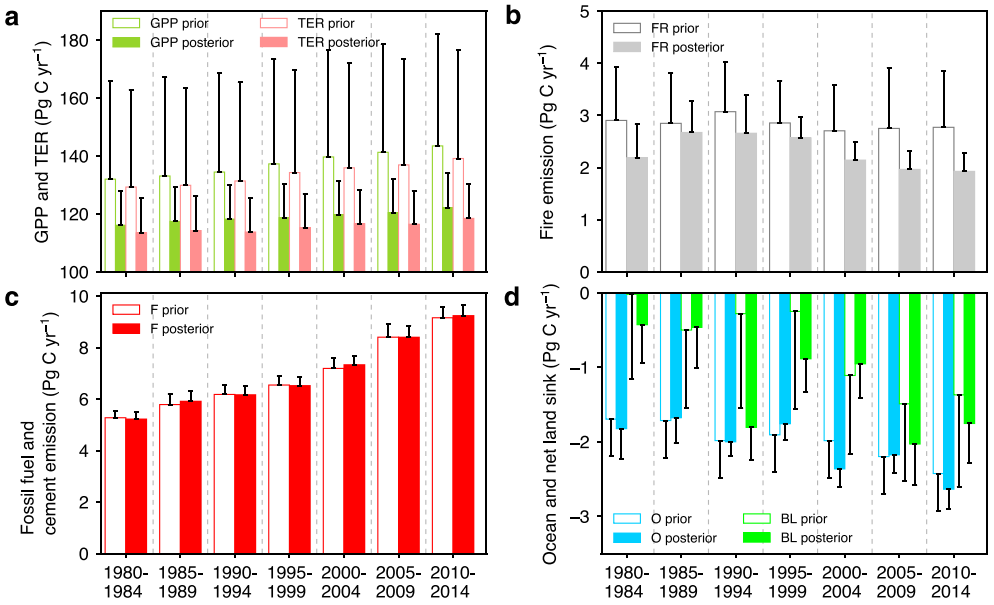

Figure 1. The prior and posterior fluxes in our optimization: (a) gross primary production (GPP, shown as reversed sign) and terrestrial ecosystem respiration (TER), (b) fire emissions (FR), (c) the fossil fuel and cement emissions (F), and (d) the ocean sink (O) and net land flux (B + L). All the fluxes given as the means of the nine tests using different combinations of LAI and GPP data sets in each 5 year period. The error bars represent the 1-σ uncertainties.

2014 using MODIS, MPI-BGC, and BESS GPP as constraints are −113 ± 11, −121 ± 11, and −123 ± 13 PgC yr^{-1}, respectively.

3.2. GPP and TER Trends

In all the nine tests, GPP and TER show a positive trend during 1980–2014 (Figure 2 and Table S5). The posterior trend of GPP is 0.18 ± 0.02 PgC yr^{-2} (mean and SD across the 9 tests), and the trend of TER is 0.16 ± 0.01 PgC yr^{-2}. The posterior trends are about half the prior trends from the DGVMs (0.40 ± 0.02 and 0.34 ± 0.02 PgC yr^{-2}, respectively, for GPP and TER). Although using different GPP observation-based data sets changes the mean values of optimized GPP and TER, it has little impact on their trends for a given LAI data set (Figure 2). By contrast, different choices of LAI data sets have a larger impact on the optimized GPP and TER trends (Table S5).

Across the nine tests, there is a significant ($p < 10^{-5}$) increase of both GPP and TER in the first and the last decade. During 1990–2004, using GIMMS LAI data produces a nearly flat GPP and a small increase of TER (Figures 2a, 2d, and 2g), while using GLASS LAI produces a persistent increase of both GPP and TER (Figures 2b, 2e, and 2h). This is mainly caused by the different relative LAI changes from these two data sets for this period (Table S3). In contrast to the prior trend, optimized TER shows a stalled growth between 1985 and 1994 (and even a decrease in five out of nine tests) and between 2000 and 2009 (Figure 2, vertical shaded areas). These periods coincide with the climate cooling that followed the Pinatubo eruption (Lucht et al., 2002) and the warming hiatus (Kosaka & Xie, 2013; Nieves et al., 2015). Five-year mean TER shows a larger temporal variability than GPP, possibly reflecting a higher sensitivity of TER to 5 year mean changes in climate. In fact, TER shows a faster rebound after each period of temperature stability or relative cooling, i.e., 0.30 ± 0.10 PgC yr^{-2} (average of the nine combinations in Figure 2) after 1990–1994 (Pinatubo) to 1995–1999 and 0.40 ± 0.07 PgC yr^{-2} after 2005–2009 (hiatus). By comparison, GPP only increased by 0.10 ± 0.12 and 0.34 ± 0.08 PgC yr^{-2} during the same intervals (Table S2). This difference between GPP and TER increase after the two 5 year periods with slower warming is significant ($p < 10^{-5}$) across the nine tests. The larger TER increases than GPP after each slower warming period results in a reduction of net land sink (see B + L values in Table S2).

3.3. Detrended Anomalies

DGVMs generally produce anomalies different from those of posterior fluxes (Figures 3a and S2). GPP anomalies from observation data sets (filled markers in Figure 3a) are within the range of posterior GPP

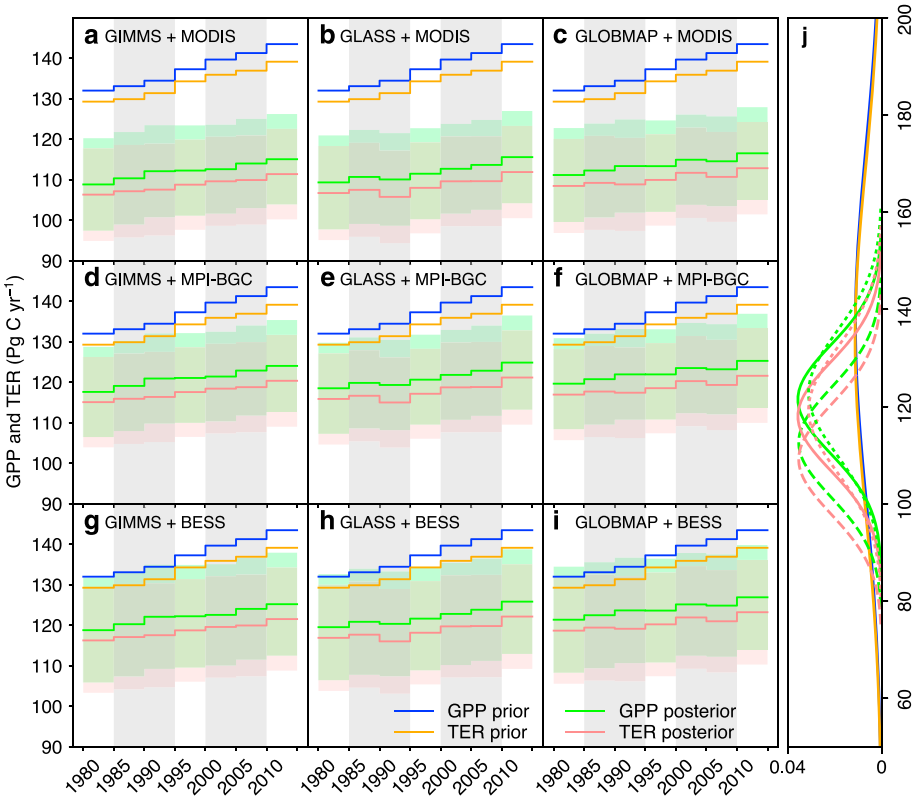

Figure 2. The prior and posterior GPP (shown as reversed sign) and TER using different combinations of LAI and GPP data sets as constraining data (a-i). The horizontal shaded areas represent the posterior uncertainties. The prior uncertainties (same as those in Figure 1a) are large and thus are not shown in a-i for better visual effects. The vertical shaded areas indicate the two slow warming periods. The probability distribution functions of prior and posterior GPP and TER (mean values over 1980–2014) are shown on the right (j). For posterior GPP and TER in j, the dashed, solid, and dotted lines indicate the optimized fluxes using MODIS, MPI-BGC, and BESS GPP, respectively, as constraints (mean values of results from three LAI data sets for each GPP data set).

anomalies except MPI-BGC GPP in 1980–1984, 1995–1999, and 2000–2004. In the early 1990s (Pinatubo eruption), B + L shows a strong enhancement (lime-colored box during 1990–1994 in Figure 3a), which we attribute mainly to a reduction of TER (strong negative anomaly) adding to a small increase of GPP (small negative anomaly with our sign convention). Note that DGVMs miss the intensified land uptake during this period, either because they do not include diffuse light effects or because the forcing data for the TRENDY project do not include the reduction in net shortwave radiation as a result of increased stratospheric aerosols from the Pinatubo eruption (Mercado et al., 2009; Roderick et al., 2001).The enhanced net land sink during 2005–2009 is also attributed to a reduced TER rather than to an increase of GPP.

We regressed anomalies of optimized GPP and TER against anomalies of climate (Figure S3) for each 5 year period. This allows to characterize quasi-decadal sensitivities of gross fluxes to climate. Despite small variations of global temperature when considering 5 year averages, a significant correlation ($p < 0.005$) was found between GPP and temperature anomalies (Figures 3b and S3a and S2b). Correlations between TER and temperature anomalies were not significant. B + L and FR did not show strong correlations with temperature for 5 year anomaly either. Anomalies of precipitation, WAI, and soil moisture do not exhibit significant correlations with either GPP or TER anomalies (Figures S3c and S3d), probably due to the compensatory water effects at biome spatial scales (Jung et al., 2017). FR anomalies are negatively correlated with soil moisture anomalies ($p < 0.05$; Figures S3e and S3f).

It looks contradictory at first glance that TER stalled during periods of decelerated warming while TER anomalies do not significantly correlate with temperature anomalies over the whole record. One possible reason is that TER also depends on biomass, litter, and soil organic carbon available from GPP of the previous years,

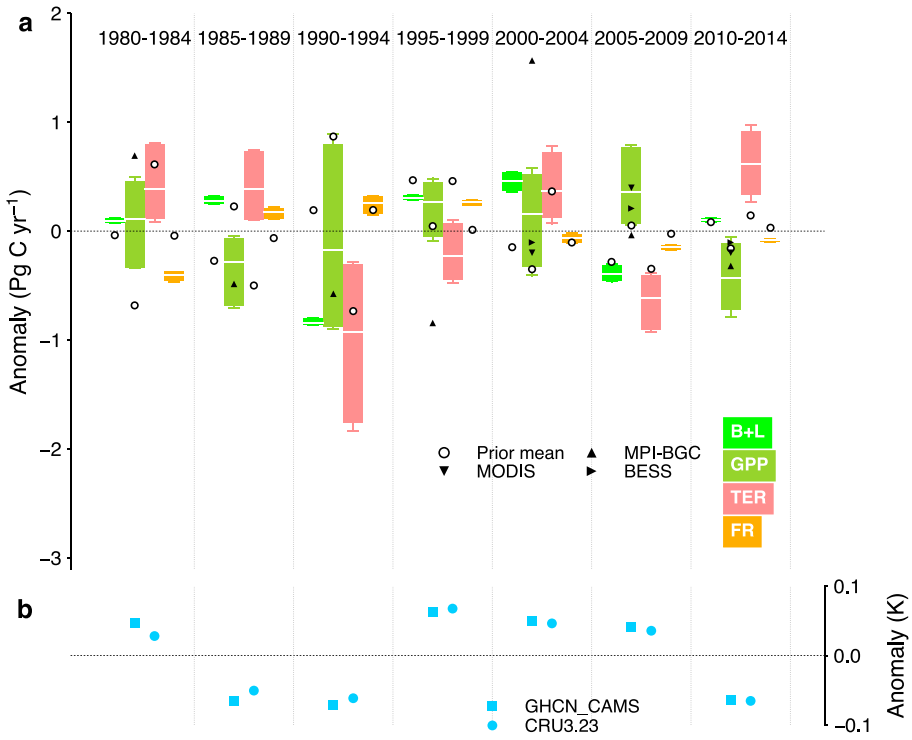

Figure 3. Detrended anomalies of (a) carbon fluxes and (b) temperature. The whisker-box plot indicates the range, interquartile, and mean of posterior values from the nine tests. Different markers represent prior mean values from TRENDY models and observation-based GPP values. Note that fluxes to the atmosphere are defined as positive, which means a negative anomaly of GPP or B + L indicating an increase of GPP and land sink while a negative anomaly of TER and FR indicating a decrease of TER and FR.

with short residence times in leaf and root pools (Malhi et al., 2011) that couple TER anomalies to GPP anomalies on a 5 year time scale. We thus conducted a multiple regression of TER anomalies against anomalies of both GPP and temperature. The regression coefficients to GPP and temperature anomalies are all significant ($p < 0.05$; Table S6). By contrast, the regression coefficients were not significant using the prior TER and GPP estimates from TRENDY models (Table S6). The R^2 of TER to GPP and temperature also improves from 0.68 using priors to 0.84 using posteriors. The coefficients of dependent variables using posterior values suggest that a reduction of TER is associated with both lower GPP anomalies and cooler temperature anomalies. These results, however, should be interpreted with caution given the small sample size ($N = 7$), the small anomalies of 5 year mean temperature, and nonrobustness across different tests (Table S6). It would also be expected that GPP and autotrophic respiration may be positively correlated in a given year, but GPP may be more highly correlated with heterotrophic respiration in subsequent years.

3.4. Sensitivity Tests

Replacing FR data sets with GFAS (Kaiser et al., 2012) and GICC (Mieville et al., 2010) increases the optimized FR by 0.25 ± 0.14 PgC yr^{-1} (mean and SD across seven 5 year periods) compared to the original nine tests but still within the uncertainty range. This sensitivity test has very small impacts on the estimates of GPP and TER and their trends (Figure S4a and Table S5). Removing the observational constraint from the soil respiration data set of Bond-Lamberty and Thomson (2010) increases the posterior trends of GPP and TER closer to the prior trends (Table S5). Although the soil respiration data seem to partly drive the inferred reduction of the trends of GPP and TER during 1980–2014, they are only critical to the change from 1990–1994 to 1995–1999. A large jump of optimized GPP and TER is found without the Bond-Lamberty and Thomson (2010) data (Figure S4b) because the relative change of GPP is not well constrained by observed LAI during this period. By contrast, the soil respiration data have little influence on the optimized GPP and TER values before 1995 and after 2000 and on the TER stalling during the relatively cooler periods of Pinatubo and

Hiatus periods (Figure S4b). The LAI data have a relatively small impact on the reduction of the overall trends from priors but determine TER stalling during the Pinatubo and Hiatus periods (Table S5 and Figure S4c). Without contributions from prior trends, the optimized trends become flat and nonsignificant (Table S5 and Figure S4d). When accounting for theoretical CO_2 effects on LUE based on Keenan et al. (2016), the trends of optimized GPP and TER during 1980–2014 increased from the original values but remained lower than the prior trends from DGVMs (Table S5 and Figure S4e). In particular, the stalling of TER during the two relatively cooler periods is robust to the inclusion of CO_2 effects on the increase of LUE (Figure S4e). Note that our theoretical estimate of the LUE sensitivity to CO_2 does not include limitations like nutrient and climate change, and thus should be cautiously interpreted. On the other hand, CO_2 effects on LAI trends modulated by climate and nutrients are implicitly included in LAI observations (for CO_2 partial contribution to LAI greening, see for instance Zhu et al., 2016).

4. Discussion

In general, the reduction in GPP and TER long-term trends compared to prior trends is driven by the soil respiration data set of Bond-Lamberty and Thomson (2010) and the relative LAI changes. Regarding quasi-decadal changes, the soil respiration data mainly constrain the change from 1990–1994 to 1995–1999 while the LAI data constrain changes during other periods. During 1990–1994 (Pinatubo eruption), we infer a stalling of TER that supports the previously reported TER reduction due to the high-latitude cooling that followed the eruption (Lucht et al., 2002). The hypothesis of higher photosynthesis from increased diffuse light fraction after the volcanic eruption (Gu et al., 2003; Mercado et al., 2009; Roderick et al., 2001) also partly explains the B + L enhancement during this period. Our findings of reduced TER during Pinatubo and warming hiatus periods are consistent with the conclusions of Keenan et al. (2016) and Ballantyne et al. (2017) using different approaches. Keenan et al. (2016) reported a slowdown in the temperature-driven ecosystem respiration during the past decade, using a satellite-driven photosynthesis-respiration model. Ballantyne et al. (2017) calculated TER as a difference of GPP and net biome productivity based on satellite and atmospheric observations and the net land sink from the global carbon budget, and also inferred a reduction of TER during the Pinatubo and the hiatus periods. They further attributed the reduction of TER to the stalling temperature and decreasing soil moisture using an empirical soil respiration model (Ballantyne et al., 2017). However, Ballantyne et al. (2017) inferred a stronger relationship between TER and temperature than between GPP and temperature on interannual time scale, which is different from our results for quasi-decadal scales. This difference may be because they calculated TER as a difference between GPP and the net land sink, while we used separate observation constraints on GPP, TER, and on other land carbon fluxes. Additionally, our study has a relatively small sample size ($N = 7$ from 1980 to 2014), and thus, all correlations regardless of significance should be interpreted with caution.

Due to differences in the observation-based GPP data sets (Table S3), optimized mean values of GPP and TER are different. By contrast, trends and quasi-decadal responses to climate are consistent between different combinations and robust to the choice of a GPP or LAI observation (Figure 2). Our results suggest that simulated trends of GPP and TER in current DGVMs are increasing too rapidly over the last three decades. However, the strong negative correlations between uncertainties in posterior GPP and TER (Figure S5) imply that current observation-based data are still inadequate evidence to fully decouple the gross fluxes of GPP and TER.

We used the relative change of LAI (growing season average) to constrain the relative change of GPP. We are aware that a change of 1% in LAI does not imply a change of 1% in GPP because a simple LUE model approximates GPP = LUE × PAR × fAPAR and fAPAR = $1 - e^{-0.5 \times \mathrm{LAI}}$ at local level (Walther et al., 2016), where PAR and fAPAR indicate photosynthetically active radiation and fraction of PAR absorbed by canopies. Even with constant LAI implying constant fAPAR, PAR trends (Dee et al., 2011) can produce GPP trends (Figure S6) although this may have minor contributions to the interannual variability of carbon fluxes (Jung et al., 2017). LUE of plant canopies may also vary over time (e.g., due to rising CO_2), which partially explains the lower posterior GPP trends than DGVMs. In the sensitivity test that accounted for the theoretical CO_2 effects causing LUE to increase, optimized GPP and TER show larger increasing trends than the original nine tests but still below DGVM priors, and the inferred TER stalling during the two relatively cooler periods is robust (Figure S4e). The growing season LUE defined as NPP/(PAR × fAPAR) from DGVMs was also found to

increase under increasing CO_2 (Thomas et al., 2016). Keenan et al. (2016) compared different drivers of GPP change and showed that indirect effects of fAPAR on GPP change during 1980–2012 diagnosed from their photosynthesis-respiration model is about half of the direct effects of CO_2 inferred from TRENDY models and water availability has little influence on GPP change (Keenan et al., 2016). However, these two approaches (Keenan et al., 2016; Thomas et al., 2016) do not necessarily match the observed CO_2 growth rate and net land sink and whether DGVMs overestimate (Kolby Smith et al., 2015) or underestimate (Thomas et al., 2016) CO_2 fertilization effects still remains uncertain. Our approach of attributing net land sink to GPP and TER, on the other hand, is fully consistent with these observations; i.e., the optimized GPP and TER are constrained not only by LAI relative trends but also by other observations like G_0 and net carbon fluxes that includes the effects of LUE changes. In addition, the correlations between annual/5 year mean GPP and growing season LAI and between relative changes of GPP and growing season LAI on any 5 year intervals are both very strong in the DGVMs (Figure S7), suggesting that growing season-integrated LAI is a good proxy of GPP. Note that we infer that this relationship between relative changes of GPP and growing season LAI is strong from DGVM result examination, but we use observations of these two quantities in the optimization, not DGVM results. The relationship between relative changes of 5 year mean GPP from MPI-BGC and LAI from GIMMS seems also linear (Figure S7c), but it should not be overinterpreted because unlike DGVMs (Figures S7a and S7b), the observation-based GPP and LAI data sets are not corresponding to each other.

A single soil respiration trend (Bond-Lamberty & Thomson, 2010) was used to constrain TER trend for the period of 1990–2010. This data set mainly poses a constraint on the relative change of TER from 1990–1994 to 1995–1999 (sensitivity test 2; Figure S4b). Global soil respiration estimated by Bond-Lamberty and Thomson (2010) (98 ± 12 PgC) accounts for about 85% of the optimized TER in our study, suggesting that the aboveground autotrophic respiration, not included in soil respiration, comprises a small fraction of the TER. To avoid the biases, we only adopted the trend rather than the absolute soil respiration value as a constraint and used a relatively larger uncertainty of this trend (Table S3). This observed soil respiration trend (0.10 PgC yr^{-2}) is also consistent with the inferred TER trend (0.11 PgC yr^{-2}) from Ballantyne et al. (2017).

Our Bayesian fusion approach constrains gross and net fluxes with various observational data sets and provides insight about multiyear variability in gross fluxes and the underlying processes that have affected the net land sink. The trends of 5 year mean GPP and TER reflect both decadal climate variability and long-term drivers such as the increasing concentration of CO_2, nitrogen deposition and changes in land use and in nutrient limitations. It is not possible with our global approach to infer which region was responsible for the stalling of TER during the two periods with a slower warming. Possible explanations for the reduced GPP and TER trends when constrained by the observations may involve either emerging biogeochemical limitations partly absent from DGVMs (e.g., reduced nitrogen deposition in some regions like North America and Europe or emerging nutrient limitations (Davidson et al., 2011; Tørseth et al., 2012)) or the slower warming at high northern latitudes especially in winter and spring (Cohen et al., 2012) resulting in both less respiration or reduced photosynthetic uptake. Combining spatially explicit observations to constrain process-based carbon cycle models, as done, e.g., in carbon cycle data assimilation systems (Peylin et al., 2016; Rayner et al., 2005) should provide more insights about the regional processes. Considering the larger sensitivity of TER than GPP to resumed future surface warming, this combination is expected to strongly reduce the sink strength of land ecosystems and would require stronger mitigation of anthropogenic emissions to keep global warming below 1.5°C.

Acknowledgments
We acknowledge the TRENDY project and TRENDY modelers for making their data available. We thank Martin Jung for providing the WAI data. CPC Soil Moisture data provided by the NOAA/OAR/ESRL PSD, Boulder, Colorado, USA, from their Web site at http://www.esrl.noaa.gov/psd/. W.L. and P.F. are supported by the European Commission-funded project LUC4C (603542). W.L., P.C., and S.Pe. acknowledge support from the European Research Council through Synergy grant ERC-2013-SyG-610028 "IMBALANCE-P." P.F. is supported by the European Union's Horizon 2020 research and innovation program, under grant agreement 641816 (CRESCENDO). J.G.C. is supported by the Earth Systems and Climate Change Hub of the Australian National Environmental Science Program. All the data supporting our study can be found in the tables in the supporting information.

References

Anav, A., Friedlingstein, P., Beer, C., Ciais, P., Harper, A., Jones, C., … Zhao, M. (2015). Spatiotemporal patterns of terrestrial gross primary production: A review. *Reviews of Geophysics*, *53*, 785–818. https://doi.org/10.1002/2015RG000483

Ballantyne, A., Smith, W., Anderegg, W., Kauppi, P., Sarmiento, J., Tans, P., … Running, S. (2017). Accelerating net terrestrial carbon uptake during the warming hiatus due to reduced respiration. *Nature Climate Change*, *7*(2), 148–152. https://doi.org/10.1038/nclimate3204

Ballantyne, A. P., Andres, R., Houghton, R., Stocker, B. D., Wanninkhof, R., Anderegg, W., … White, J. W. C. (2015). Audit of the global carbon budget: Estimate errors and their impact on uptake uncertainty. *Biogeosciences*, *12*(8), 2565–2584. https://doi.org/10.5194/bg-12-2565-2015

Beer, C., Reichstein, M., Tomelleri, E., Ciais, P., Jung, M., Carvalhais, N., … Papale, D. (2010). Terrestrial gross carbon dioxide uptake: Global distribution and covariation with climate. *Science*, *329*(5993), 834–838. https://doi.org/10.1126/science.1184984

Best, M. J., Pryor, M., Clark, D. B., Rooney, G. G., Essery, R. L. H., Ménard, C. B., … Harding, R. J. (2011). The Joint UK Land Environment Simulator (JULES), model description—Part 1: Energy and water fluxes. *Geoscientific Model Development*, *4*(3), 677–699. https://doi.org/10.5194/gmd-4-677-2011

Betts, R. A., Jones, C. D., Knight, J. R., Keeling, R. F., & Kennedy, J. J. (2016). El Niño and a record CO_2 rise. *Nature Climate Change*, *6*(9), 806–810. https://doi.org/10.1038/nclimate3063

Bond-Lamberty, B., & Thomson, A. (2010). Temperature-associated increases in the global soil respiration record. *Nature*, *464*(7288), 579–582. https://doi.org/10.1038/nature08930

Ciais, P., Sabine, C., Bala, G., Bopp, L., Brovkin, V., Canadell, J., … Thornton, P. (2013). 2013: Carbon and other biogeochemical cycles. In T. F. Stocker, et al. (Eds.), *Climate Change 2013 – The Physical Science Basis Working Group I Contribution to the Fifth Assessment Report of the Intergovernmental Panel on Climate Change* (pp. 465–570). Cambridge, United Kingdom and New York: Cambridge University Press. https://doi.org/10.1017/CBO9781107415324.015

Clark, D. B., Mercado, L. M., Sitch, S., Jones, C. D., Gedney, N., Best, M. J., … Cox, P. M. (2011). The Joint UK Land Environment Simulator (JULES), model description – Part 2: Carbon fluxes and vegetation dynamics. *Geoscientific Model Development*, *4*(3), 701–722. https://doi.org/10.5194/gmd-4-701-2011

Cohen, J. L., Furtado, J. C., Barlow, M., Alexeev, V. A., & Cherry, J. E. (2012). Asymmetric seasonal temperature trends. *Geophysical Research Letters*, *39*, L04705. https://doi.org/10.1029/2011GL050582

Davidson, E. A., David, M. B., Galloway, J. N., Goodale, C. L., Haeuber, R., Harrison, J. A., … Peel, J. L. (2011). Excess nitrogen in the U.S. environment: Trends, risks, and solutions, *Issues Ecol.*, (15).

Dee, D., Uppala, S., Simmons, A., Berrisford, P., Poli, P., Kobayashi, S., … Bauer, P. (2011). The ERA-Interim reanalysis: Configuration and performance of the data assimilation system. *Quaterly Journal of the Royal Meteorological Society*, *137*(656), 553–597. https://doi.org/10.1002/qj.828

Dorigo, W. A., Scipal, K., Parinussa, R. M., Liu, Y. Y., Wagner, W., De Jeu, R. A. M., & Naeimi, V. (2010). Error characterisation of global active and passive microwave soil moisture datasets. *Hydrology and Earth System Sciences*, *14*(12), 2605–2616. https://doi.org/10.5194/hess-14-2605-2010

Duveiller, G., & Cescatti, A. (2016). Spatially downscaling Sun-induced chlorophyll fluorescence leads to an improved temporal correlation with gross primary productivity. *Remote Sensing of Environment*, *182*, 72–89. https://doi.org/10.1016/j.rse.2016.04.027

Fan, Y., & van den Dool, H. (2004). Climate Prediction Center global monthly soil moisture data set at 0.5 degree resolution for 1948 to present. *Journal of Geophysical Research*, *109*, D10102. https://doi.org/10.1029/2003JD004345

Fan, Y., & van den Dool, H. (2008). A global monthly land surface air temperature analysis for 1948-present. *Journal of Geophysical Research*, *113*, D01103. https://doi.org/10.1029/2007JD008470

Frankenberg, C., Fisher, J. B., Worden, J., Badgley, G., Saatchi, S. S., Lee, J. E., … Yokota, T. (2011). New global observations of the terrestrial carbon cycle from GOSAT: Patterns of plant fluorescence with gross primary productivity. *Geophysical Research Letters*, *38*, L17706. https://doi.org/10.1029/2011GL048738

Giglio, L., Randerson, J. T., & van der Werf, G. R. (2013). Analysis of daily, monthly, and annual burned area using the fourth-generation global fire emissions database (GFED4). *Journal of Geophysical Research: Biogeosciences*, *118*, 317–328. https://doi.org/10.1002/jgrg.20042

Gu, L., Baldocchi, D. D., Wofsy, S. C., Munger, J. W., Michalsky, J. J., Urbanski, S. P., & Boden, T. A. (2003). Response of a deciduous forest to the Mount Pinatubo eruption: Enhanced photosynthesis. *Science*, *299*(5615), 2035–2038. https://doi.org/10.1126/science.1078366

Guanter, L., Frankenberg, C., Dudhia, A., Lewis, P. E., Gómez-Dans, J., Kuze, A., … Grainger, R. G. (2012). Retrieval and global assessment of terrestrial chlorophyll fluorescence from GOSAT space measurements. *Remote Sensing of Environment*, *121*, 236–251. https://doi.org/10.1016/j.rse.2012.02.006

Harris, I., Jones, P. D., Osborn, T. J., & Lister, D. H. (2014). Updated high-resolution grids of monthly climatic observations - the CRU TS3.10 dataset. *International Journal of Climatology*, *34*(3), 623–642. https://doi.org/10.1002/joc.3711

Heil, A., Kaiser, J. W., Van der Werf, G. R., Wooster, M. J., Schultz, M. G., & van der Gon, H. D. (2010). Assessment of the real-time fire emissions (GFASv0) by MACC, European Centre for Medium-Range Weather Forecasts.

Huang, M., Piao, S., Sun, Y., Ciais, P., Cheng, L., Mao, J., … Wang, Y. (2015). Change in terrestrial ecosystem water-use efficiency over the last three decades. *Global Change Biology*, *21*(6), 2366–2378. https://doi.org/10.1111/gcb.12873

Ito, A., & Inatomi, M. (2012). Use of a process-based model for assessing the methane budgets of global terrestrial ecosystems and evaluation of uncertainty. *Biogeosciences*, *9*(2), 759–773. https://doi.org/10.5194/bg-9-759-2012

Jacobson, A. R., Fletcher, S. E. M., Gruber, N., Sarmiento, J. L., & Gloor, M. (2007). A joint atmosphere-ocean inversion for surface fluxes of carbon dioxide: 1. Methods and global-scale fluxes. *Global Biogeochemical Cycles*, *21*, GB1019. https://doi.org/10.1029/2005GB002556

Jain, A., & Yang, X. (2005). Modeling the effects of two different land cover change data sets on the carbon stocks of plants and soils in concert with {CO_2} and climate change. *Global Biogeochemical Cycles*, *19*, GB2015. https://doi.org/10.1029/2004GB002349

Jiang, C., & Ryu, Y. (2016). Multi-scale evaluation of global gross primary productivity and evapotranspiration products derived from Breathing Earth System Simulator (BESS). *Remote Sensing of Environment*, *186*, 528–547. https://doi.org/10.1016/j.rse.2016.08.030

Joiner, J., Guanter, L., Lindstrot, R., Voigt, M., Vasilkov, A. P., Middleton, E. M., … Frankenberg, C. (2013). Global monitoring of terrestrial chlorophyll fluorescence from moderate spectral resolution near-infrared satellite measurements: Methodology, simulations, and application to GOME-2. *Atmospheric Measurement Techniques Discussions*, *6*(2), 3883–3930. https://doi.org/10.5194/amtd-6-3883-2013

Jung, M., Reichstein, M., Margolis, H. A., Cescatti, A., Richardson, A. D., Arain, M. A., … Williams, C. (2011). Global patterns of land-atmosphere fluxes of carbon dioxide, latent heat, and sensible heat derived from eddy covariance, satellite, and meteorological observations. *Journal of Geophysical Research*, *116*, G00J07. https://doi.org/10.1029/2010JG001566

Jung, M., Reichstein, M., Schwalm, C. R., Huntingford, C., Sitch, S., Ahlström, A., … Zeng, N. (2017). Compensatory water effects link yearly global land CO_2 sink changes to temperature. *Nature*, *541*(7638), 516–520. https://doi.org/10.1038/nature20780

Kaiser, J. W., Heil, A., Andreae, M. O., Benedetti, A., Chubarova, N., Jones, L., … van der Werf, G. R. (2012). Biomass burning emissions estimated with a global fire assimilation system based on observed fire radiative power. *Biogeosciences*, *9*(1), 527–554. https://doi.org/10.5194/bg-9-527-2012

Kato, E., Kinoshita, T., Ito, A., Kawamiya, M., & Yamagata, Y. (2013). Evaluation of spatially explicit emission scenario of land-use change and biomass burning using a process-based biogeochemical model. *Journal Land Use Science*, *8*(1), 104–122. https://doi.org/10.1080/1747423X.2011.628705

Keeling, R. F., & Manning, A. C. (2014). Studies of recent changes in atmospheric O_2 content. In H. D. Holland & K. K. Turekian (Eds.), *Treatise on Geochemistry* (2nd ed., pp. 385–404). Oxford: Elsevier. https://doi.org/10.1016/B978-0-08-095975-7.00420-4

Keenan, T. F., Prentice, I. C., Canadell, J. G., Williams, C., Wang, H., Raupach, M. R., & Collatz, G. J. (2016). Recent pause in the growth rate of atmospheric CO_2 due to enhanced terrestrial carbon uptake. *Nature Communications*, 1–9. https://doi.org/10.1038/ncomms13428

Khatiwala, S., Primeau, F., & Hall, T. (2009). Reconstruction of the history of anthropogenic CO_2 concentrations in the ocean. *Nature*, *462*(7271), 346–349. https://doi.org/10.1038/nature08526

Kolby Smith, W., Reed, S. C., Cleveland, C. C., Ballantyne, A. P., Anderegg, W. R. L., Wieder, W. R., … Running, S. W. (2015). Large divergence of satellite and Earth system model estimates of global terrestrial CO_2 fertilization. *Nature Climate Change*, *6*(3), 306–310. https://doi.org/10.1038/nclimate2879

Kosaka, Y., & Xie, S.-P. (2013). Recent global-warming hiatus tied to equatorial Pacific surface cooling. *Nature*, *501*(7467), 403–407. https://doi.org/10.1038/nature12534

Krinner, G., Viovy, N., de Noblet-Ducoudré, N., Ogée, J., Polcher, J., Friedlingstein, P., … Prentice, C. I. (2005). A dynamic global vegetation model for studies of the coupled atmosphere-biosphere system. *Global Biogeochemical Cycles*, *19*, GB1015. https://doi.org/10.1029/2003GB002199

Landschützer, P., Gruber, N., Bakker, D. C. E., & Schuster, U. (2014). Recent variability of the global ocean carbon sink. *Global Biogeochemical Cycles*, *28*, 927–949. https://doi.org/10.1002/2014GB004853

Le Quéré, C., Moriarty, R., Andrew, R. M., Peters, G. P., Ciais, P., Friedlingstein, P., & Jones, S. D. (2015). Global carbon budget 2014. *Earth System Science Data*, *7*(1), 47–85. https://doi.org/10.5194/essd-7-47-2015

Li, W., Ciais, P., Wang, Y., Peng, S., Broquet, G., Ballantyne, A. P., … Le Quéré, C. (2016). Reducing uncertainties in decadal variability of the global carbon budget with multiple datasets. *Proceedings of the National Academy of Sciences*, *113*(46), 13,104–13,108. https://doi.org/10.1073/pnas.1603956113

Liu, Y., Liu, R., & Chen, J. M. (2012). Retrospective retrieval of long-term consistent global leaf area index (1981–2011) from combined AVHRR and MODIS data. *Journal of Geophysical Research*, *117*, G04003. https://doi.org/10.1029/2012JG002084

Lucht, W., Prentice, I. C., Myneni, R. B., Sitch, S., Friedlingstein, P., Cramer, W., … Smith, B. (2002). Climatic control of the high-latitude vegetation greening trend and Pinatubo effect. *Science*, *296*(5573), 1687–1689. https://doi.org/10.1126/science.1071828

Luo, Y., Ahlström, A., Allison, S. D., Batjes, N. H., Brovkin, V., Carvalhais, N., … Zhou, T. (2016). Toward more realistic projections of soil carbon dynamics by Earth system models. *Global Biogeochemical Cycles*, *30*, 40–56. https://doi.org/10.1002/2015GB005239

Malhi, Y., Doughty, C., & Galbraith, D. (2011). The allocation of ecosystem net primary productivity in tropical forests. *Philosophical Transactions of the Royal Society B: Biological Sciences*, *366*(1582), 3225–3245. https://doi.org/10.1098/rstb.2011.0062

McNeil, B. I., Matear, R. J., Key, R. M., Bullister, J. L., & Sarmiento, J. L. (2003). Anthropogenic CO_2 uptake by the ocean based on the global chlorofluorocarbon data set. *Science*, *299*(5604), 235–239. https://doi.org/10.1126/science.1077429

Mercado, L. M., Bellouin, N., Sitch, S., Boucher, O., Huntingford, C., Wild, M., & Cox, P. M. (2009). Impact of changes in diffuse radiation on the global land carbon sink. *Nature*, *458*(7241), 1014–1017. https://doi.org/10.1038/nature07949

Mieville, A., Granier, C., Liousse, C., Guillaume, B., Mouillot, F., Lamarque, J.-F., … Pétron, G. (2010). Emissions of gases and particles from biomass burning during the 20th century using satellite data and an historical reconstruction. *Atmospheric Environment*, *44*(11), 1469–1477. https://doi.org/10.1016/j.atmosenv.2010.01.011

Nieves, V., Willis, J. K., & Patzert, W. C. (2015). Recent hiatus caused by decadal shift in indo-Pacific heating. *Science*, *349*(6247), 532–535. https://doi.org/10.1126/science.aaa4521

NOAA/ESRL (2015). NOAA/ESRL calculation of global means. Retrieved from http://www.esrl.noaa.gov/gmd/ccgg/about/global_means.html (Accessed 9 August 2015)

Oleson, K. W., Lawrence, D. M., Bonan, G. B., Drewniak, B., Huang, M., Koven, C. D., … Thornton, P. E. (2013). Technical description of version 4.5 of the Community Land Model (CLM).

Pan, Y., Birdsey, R. A., Fang, J., Houghton, R., Kauppi, P. E., Kurz, W. A., … Hayes, D. (2011). A large and persistent carbon sink in the world's forests. *Science*, *333*(6045), 988–993. https://doi.org/10.1126/science.1201609

Peylin, P., Bacour, C., MacBean, N., Leonard, S., Rayner, P. J., Kuppel, S., … Prunet, P. (2016). A new step-wise carbon cycle data assimilation system using multiple data streams to constrain the simulated land surface carbon cycle. *Geoscientific Model Development Discussion*, 1–52. https://doi.org/10.5194/gmd-2016-13

Rayner, P. J., Scholze, M., Knorr, W., Kaminski, T., Giering, R., & Widmann, H. (2005). Two decades of terrestrial carbon fluxes from a carbon cycle data assimilation system (CCDAS). *Global Biogeochemical Cycles*, *19*, GB2026. https://doi.org/10.1029/2004GB002254

Reick, C. H., Raddatz, T., Brovkin, V., & Gayler, V. (2013). Representation of natural and anthropogenic land cover change in MPI-ESM. *Journal of Advances in Modeling Earth Systems*, *5*(3), 459–482. https://doi.org/10.1002/jame.20022

Rödenbeck, C., Bakker, D. C. E., Gruber, N., Iida, Y., Jacobson, A. R., Jones, S., … Zeng, J. (2015). Data-based estimates of the ocean carbon sink variability—First results of the Surface Ocean pCO_2 Mapping intercomparison (SOCOM). *Biogeosciences*, *12*(23), 7251–7278. https://doi.org/10.5194/bg-12-7251-2015

Rödenbeck, C., Bakker, D. C. E., Metzl, N., Olsen, A., Sabine, C., Cassar, N., … Heimann, M. (2014). Interannual sea–air CO_2 flux variability from an observation-driven ocean mixed-layer scheme. *Biogeosciences*, *11*(17), 4599–4613. https://doi.org/10.5194/bg-11-4599-2014

Rödenbeck, C., Keeling, R. F., Bakker, D. C. E., Metzl, N., Olsen, A., Sabine, C., & Heimann, M. (2013). Global surface-ocean pCO_2 and sea–air CO_2 flux variability from an observation-driven ocean mixed-layer scheme. *Ocean Science*, *9*(2), 193–216. https://doi.org/10.5194/os-9-193-2013

Roderick, M., Farquhar, G., Berry, S., & Noble, I. (2001). On the direct effect of clouds and atmospheric particles on the productivity and structure of vegetation. *Oecologia*, *129*(1), 21–30. https://doi.org/10.1007/s004420100760

Schultz, M. G., Heil, A., Hoelzemann, J. J., Spessa, A., Thonicke, K., Goldammer, J. G., … van het Bolscher, M. (2008). Global wildland fire emissions from 1960 to 2000. *Global Biogeochemical Cycles*, *22*, GB2002. https://doi.org/10.1029/2007GB003031

Sitch, S., Friedlingstein, P., Gruber, N., Jones, S. D., Murray-Tortarolo, G., Ahlström, A., … Myneni, R. (2015). Recent trends and drivers of regional sources and sinks of carbon dioxide. *Biogeosciences*, *12*(3), 653–679. https://doi.org/10.5194/bg-12-653-2015

Sitch, S., Smith, B., Prentice, I. C., Arneth, A., Bondeau, A., Cramer, W., … Venevsky, S. (2003). Evaluation of ecosystem dynamics, plant geography and terrestrial carbon cycling in the LPJ dynamic global vegetation model. *Global Change Biology*, *9*(2), 161–185. https://doi.org/10.1046/j.1365-2486.2003.00569.x

Smith, B., Prentice, I. C., & Sykes, M. T. (2001). Representation of vegetation dynamics in the modelling of terrestrial ecosystems: Comparing two contrasting approaches within European climate space. *Global Ecology and Biogeography*, *10*(6), 621–637. https://doi.org/10.1046/j.1466-822X.2001.00256.x

Steinkamp, K., & Gruber, N. (2013). A joint atmosphere-ocean inversion for the estimation of seasonal carbon sources and sinks. *Global Biogeochemical Cycles*, *27*, 732–745. https://doi.org/10.1002/gbc.20064

Stocker, B. D., Feissli, F., Strassmann, K. M., Spahni, R., & Joos, F. (2014). Past and future carbon fluxes from land use change, shifting cultivation and wood harvest. *Tellus B*, *66*(1). https://doi.org/10.3402/tellusb.v66.23188

Tarantola, A. (2005). *Inverse problem theory and methods for model parameter estimation*. Philadelphia: SIAM. https://doi.org/10.1137/1.9780898717921

Thomas, R. T., Prentice, I. C., Graven, H., Ciais, P., Fisher, J. B., Hayes, D. J., … Zeng, N. (2016). Increased light-use efficiency in northern terrestrial ecosystems indicated by CO_2 and greening observations. *Geophysical Research Letters*, *43*, 11,339–11,349. https://doi.org/10.1002/2016GL070710

Tørseth, K., Aas, W., Breivik, K., Fjæraa, A. M., Fiebig, M., Hjellbrekke, A. G., … Yttri, K. E. (2012). Introduction to the European Monitoring and Evaluation Programme (EMEP) and observed atmospheric composition change during 1972–2009. *Atmospheric Chemistry and Physics*, *12*(12), 5447–5481. https://doi.org/10.5194/acp-12-5447-2012

Tramontana, G., Jung, M., Schwalm, C. R., Ichii, K., Camps-Valls, G., Ráduly, B., … Papale, D. (2016). Predicting carbon dioxide and energy fluxes across global FLUXNET sites with regression algorithms. *Biogeosciences*, *13*(14), 4291–4313. https://doi.org/10.5194/bg-13-4291-2016

Van Der Werf, G. R., Randerson, J. T., Giglio, L., Collatz, G. J., Mu, M., Kasibhatla, P. S., … Van Leeuwen, T. T. (2010). Global fire emissions and the contribution of deforestation, savanna, forest, agricultural, and peat fires (1997-2009). *Atmospheric Chemistry and Physics*, *10*(23), 11,707–11,735. https://doi.org/10.5194/acp-10-11707-2010

Walther, S., Voigt, M., Thum, T., Gonsamo, A., Zhang, Y., Köhler, P., … Guanter, L. (2016). Satellite chlorophyll fluorescence measurements reveal large-scale decoupling of photosynthesis and greenness dynamics in boreal evergreen forests. *Global Change Biology*, *22*(9), 2979–2996. https://doi.org/10.1111/gcb.13200

Xiao, Z., Liang, S., Wang, J., Chen, P., Yin, X., Zhang, L., & Song, J. (2014). Use of general regression neural networks for generating the GLASS leaf area index product from time-series MODIS surface reflectance. *IEEE Transactions on Geoscience and Remote Sensing*, *52*(1), 209–223. https://doi.org/10.1109/TGRS.2013.2237780

Zaehle, S., & Friend, A. D. (2010). Carbon and nitrogen cycle dynamics in the O-CN land surface model: 1. Model description, site-scale evaluation, and sensitivity to parameter estimates. *Global Biogeochemical Cycles*, *24*, GB1005. https://doi.org/10.1029/2009GB003521

Zeng, N., Mariotti, A., & Wetzel, P. (2005). Terrestrial mechanisms of interannual CO_2 variability. *Global Biogeochemical Cycles*, *19*, GB1016. https://doi.org/10.1029/2004GB002273

Zhao, M., Heinsch, F. A., Nemani, R. R., & Running, S. W. (2005). Improvements of the MODIS terrestrial gross and net primary production global data set. *Remote Sensing of Environment*, *95*(2), 164–176. https://doi.org/10.1016/j.rse.2004.12.011

Zhao, M., Running, S. W., & Nemani, R. R. (2006). Sensitivity of Moderate Resolution Imaging Spectroradiometer (MODIS) terrestrial primary production to the accuracy of meteorological reanalyses. *Journal of Geophysical Research*, *111*, G01002. https://doi.org/10.1029/2004JG000004

Zhu, Z., Bi, J., Pan, Y., Ganguly, S., Anav, A., Xu, L., … Myneni, R. (2013). Global data sets of vegetation leaf area index (LAI)3g and fraction of photosynthetically active radiation (FPAR)3g derived from Global Inventory Modeling and Mapping Studies (GIMMS) normalized difference vegetation index (NDVI3g) for the period 1981 to 2. *Remote Sensing*, *5*(2), 927–948. https://doi.org/10.3390/rs5020927

Zhu, Z., Piao, S., Myneni, R. B., Huang, M., Zeng, Z., Canadell, J. G., … Zeng, N. (2016). Greening of the Earth and its drivers. *Nature Climate Change*, *6*(8), 791–795. https://doi.org/10.1038/nclimate3004